doi:10.26443/seismica.v4i1.1453

Delineation of 3D Crustal Seismic Structures Beneath Western Tibet and the Himalayan Range Using Local Earthquake Tomography

Arghya Kusum Dey[1,2], **Niptika Jana** * [1], **Rahul Biswas**[2]

[1]Department of Applied Geophysics, Indian Institute of Technology (Indian School of Mines) Dhanbad, Dhanbad, India, [2]CSIR-National Geophysical Research Institute, Hyderabad, India

Author contributions: *Conceptualization*: Niptika Jana. *Validation*: Arghya Kusum Dey, Niptika Jana. *Formal Analysis*: Arghya Kusum Dey. *Resources*: Niptika Jana, Rahul Biswas. *Writing - Original draft*: Arghya Kusum Dey, Niptika Jana. *Writing - Review & Editing*: Arghya Kusum Dey, Niptika Jana, Rahul Biswas. *Visualization*: Arghya Kusum Dey, Niptika Jana. *Supervision*: Niptika Jana, Rahul Biswas.

Abstract This study aims to image the crustal structure of the western Tibetan Plateau by analyzing the velocity structure of elastic waves, using manually picked P- and S-wave arrival times from waveform data recorded by temporarily installed seismic stations in western Tibet. Preliminary events located using the VELEST algorithm resulted in the development of a 1-D velocity model through inversion, which was then used in the TomoDD algorithm to relocate earthquakes and generate a high-resolution 3-D velocity structure model. A significant number of events were located between the Karakoram fault (KKF), Main Boundary Thrust, and Main Central Thrust. A low P-wave anomaly of approximately ∼8% is noted in the vicinity of the KKF, while a significant low P-wave anomaly is also observed in the crust beneath the western margin. A low P-wave anomaly is concentrated beneath the Lhasa block, whereas a relatively higher P-wave anomaly is evident in the Himalayan terrane. The KKF dips beneath the Tibetan plateau towards the northeast. Evidence of partial melting in the crust beneath the Tibetan plateau and mid-crustal channel flow of slower crustal material from the plateau towards the Himalayan range can also be delineated through the observed velocity structures found in the study.

Production Editor:
Yen Joe Tan
Handling Editor:
Chiara Civiero
Copy & Layout Editor:
Théa Ragon

Received:
September 18, 2024
Accepted:
May 26, 2025
Published:
June 13, 2025

1 Introduction

The Tibetan Plateau has formed as the Indian and Eurasian plates have converged since the early Eocene (Yin and Harrison, 2000; Royden et al., 2008). Spanning up to 2.5 million square kilometers with an average elevation exceeding 4500 metres, it is the highest plateau in the world, situated at the intersection of Central, East, and South Asia (Molnar and Tapponnier, 1975; Yin and Harrison, 2000). Research indicates that the plateau's paleo-elevation was approximately 3000 m during the early Miocene. From 25.5 to 21.6 Ma, there was an average decrease of 900 m in elevation, followed by a subsequent rise of 500 to 1000 m from 21.6 to 20.4 Ma (Jia, 2015). The ongoing plate collision has resulted in a crustal thickness of 60-80 km (Yin and Harrison, 2000; Bilham et al., 2004). The boundary between the Indian and Eurasian plates is one of the most seismically active regions in the Himalayan terrane. Over the past century, this area has experienced numerous significant earthquakes, including the M7.1 Tingri earthquake in 2025, the M7.8 Nepal earthquake in 2015, the M6.9 Sikkim earthquake in 2011, the M7.6 Kashmir earthquake in 2005, the M6.6 Chamoli earthquake in 1999, the M6.8 Uttarkashi earthquake in 1991, and the M8.1 Bihar earthquake in 1934. These earthquakes predominantly occurred in the western and southern regions adjacent to Tibet, indicating that major seismic events are common at the edge of the Tibetan Plateau. Today, the Tibetan Plateau extends from the Tarim Basin and Kunlun Shan in the north to the Himalayan Mountain range in the south. The plateau comprises three main blocks: the Songpan-Ganzi block, the Qiangtang block, and the Lhasa block. These blocks lie on a Precambrian continental crust that dates back at least one billion years. Before the Late Paleozoic era, the Lhasa and Qiangtang blocks were part of the Gondwana supercontinent (Kapp et al., 2003, 2007).

Our study focuses on the Himalayas, Lhasa, and Qiangtang terrane at the western edge of the Tibetan plateau (Fig. 1), which are distinguished by various sutures and faults formed in different tectonic contexts over time (Yin and Harrison, 2000; Kapp et al., 2005). Key geological features in this area include the Bangong–Nujiang Suture (BNS), the Indus-Yarlung Suture (IYS), and the Karakoram Fault (KKF) (Fig. 1). Western Tibet is characterized by two main geological blocks: the Lhasa block, with a width of 300 km and length 200 km (Yin and Harrison, 2000; Kapp et al., 2005) and the 500–600 km wide Qiangtang block (Fig. 1). Geographically, the Lhasa block is the southernmost part of the Tibetan Plateau. The Qiangtang block lies to the north of the BNS and extends up to the Jinsa Suture zone to the north (Biswas and Singh, 2020b; Murphy et al., 1997;

*Corresponding author: niptika.jana.1201@gmail.com

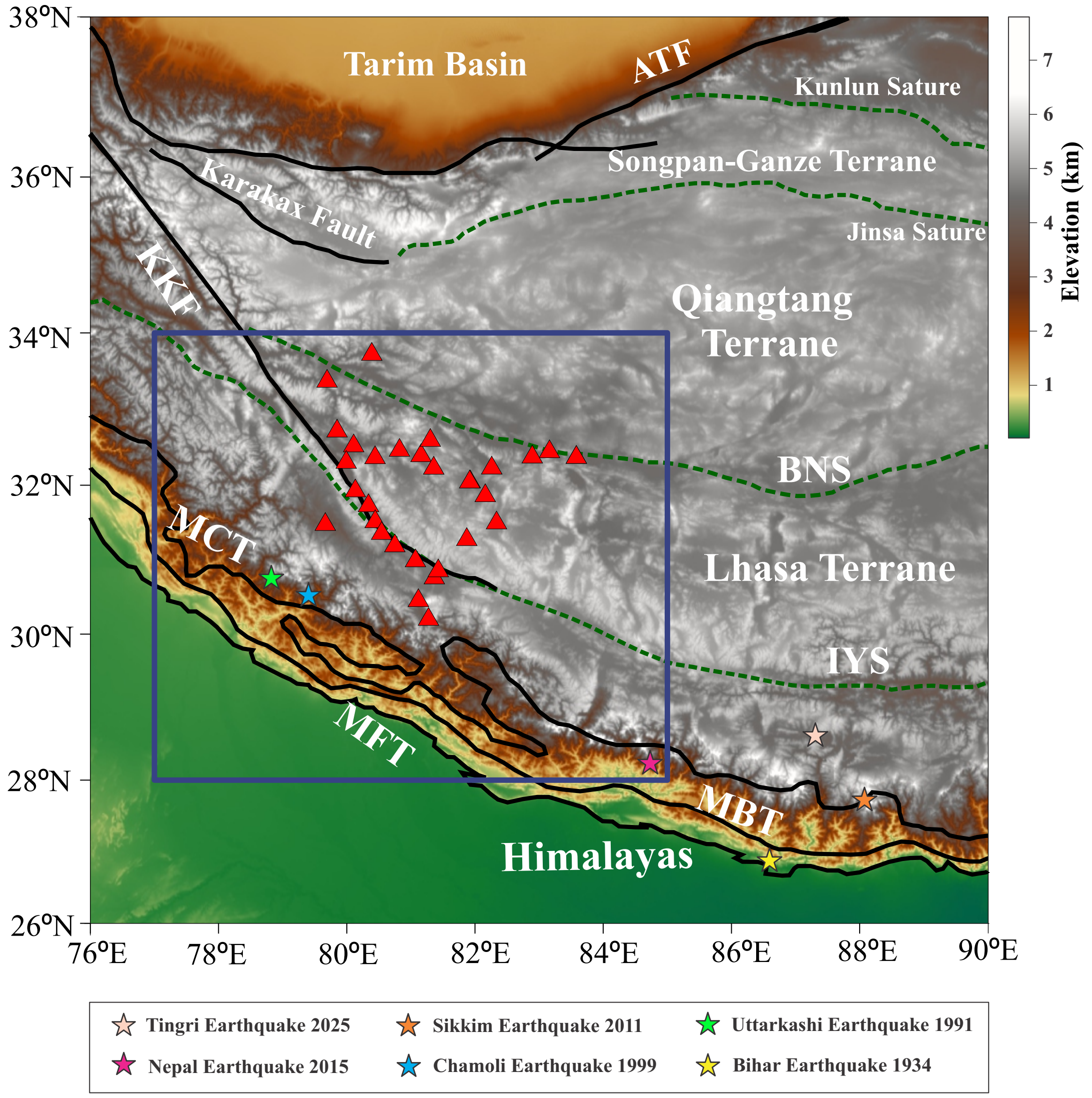

Figure 1 Station map of the seismic network (see red triangles) across the western Tibet. The green dotted lines and black lines denote significant sutures and faults, respectively, transecting the study area as indicated in the map, with the blue rectangle representing the specific area of interest. The most significant earthquakes have been mentioned in the figure. Major earthquakes that occurred across/adjacent to the study area have also been represented.

Yin and Harrison, 2000). To the west, the KKF forms the boundary of the Qiangtang block. The KKF is a dextral strike-slip fault, that developed during the early Miocene to Pliocene epochs (Valli et al., 2007), stretching ~700 km and intersecting with the IYS at its southern end (Fig. 1). The northern boundary of the Lhasa block is defined by the BNS, which separates it from the Qiangtang block and from the Tethys Himalaya across the IYS, and is also known as the Yarlung-Zangbo Suture.

Despite extensive research conducted over the past 40 years across the Tibetan plateau using various methods, including GPS surveys, gravity measurements, controlled-source seismic surveys, and magnetotelluric surveys (Shen et al., 2005; Basuyau et al., 2013; Klemperer, 2006; Alsdorf et al., 1998), the crustal structure of western Tibet remains less well understood compared to its eastern and southern regions. Previous studies report that crustal thickness varies from 26 to 88 km across the Indian Shield and the Himalayan-Eurasian subduction belt (Singh et al., 2017, 2015; Yuan et al., 1997), while the Moho depth beneath the western Himalayas and Tibet is reported to be around 70–75 km (Biswas and Singh, 2020b; Razi et al., 2014). Despite the prior seismological studies across this area—such as receiver function analysis (Wittlinger et al., 2004), ambient noise analysis (Gilligan et al., 2015), Lg/Pg attenuation tomography (Jaiswal et al., 2020, 2022), body and coda wave attenuation (Biswas and Singh, 2020b,a), and velocity tomography (Razi et al., 2014, 2016)—significant gaps in understanding the crustal structure of the western Tibet, especially across the KKF persists. While Razi et al. (2014) provided excellent insights into the crust beneath the Lhasa block and Qiangtang block, their efforts yielded poor results in resolving the crust in the region south of the KKF and the Himalayan terrane. This discrepancy may be due to the fact that the study used regional earthquake hypocenters, located in the northern Qiangtang block and the neighboring southern margin of the Tarim basin. This created a wide scope for probing the crustal velocity structure beneath the Hi-

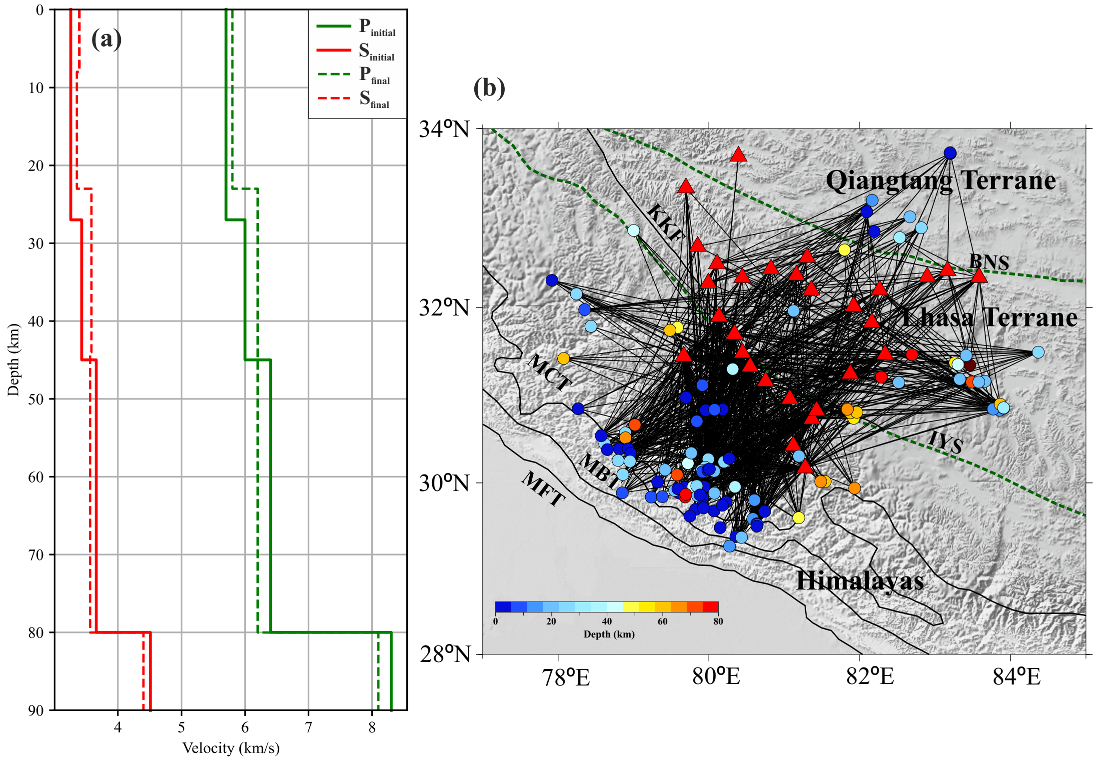

Figure 2 (a) Solid line represents the initial 1D Vp and Vs velocity used for the Velest analysis, dotted line represents the final 1D Vp and Vs velocity used as the input for velocity inversion in tomoDD algorithm. (b) Raypaths from earthquake epicenter to the seismic station are depicted by black lines; the hypocentral depth of the earthquakes are represented using the colorbar attached below.

malayan terrane and the southern edge of western Tibet, which our present observations fulfill.

Our study focuses on the local earthquake tomography to provide a deeper insight into the region, especially focusing on the KKF. The role of the KKF remains contentious, with some researchers (Razi et al., 2014; Klemperer et al., 2013) suggesting it acts as a barrier to material transport, while others (Gilligan et al., 2015) argue the opposite. The fraction of Indian lithosphere still present in the upper mantle beneath Tibet is a matter of debate, particularly in the western region where data is sparse and imaging is less clear. There is significant support for the idea that pre-existing Asian lithosphere is present beneath northern Tibet (Kind et al., 1996; Wittlinger et al., 2004; Nábělek et al., 2009); however, the presence of coherent mantle lithosphere in eastern Tibet is disputed (Dubey et al., 2022).

Examining the configuration of the former Indian lithosphere beneath Tibet, provides not only valuable insights into the geodynamic history of the India-Asia collision but also serves as a critical test for broader theories on the rheology of continental lithosphere. This study focuses on understanding the seismic structure of the Indian lithosphere as it descends beneath western Tibet. To achieve this, local earthquake tomography and relocation techniques are employed to model the 3-D P-wave and S-wave velocity structure, using data collected from a spatially distributed seismic array that operated across western Tibet between 2007 and 2011. Local earthquake data offer significant advantages over teleseismic data, as inversion of teleseismic data for crustal structure typically involves higher frequencies and larger incident angles. Therefore, in regions of high seismicity, the upper crustal architecture can be effectively studied from multiple directions by installing a seismic network (Kissling, 1988). The Local Earthquake Tomography studies also often emphasize the importance of precise hypocenter locations for creating reliable models. Traditionally, this has been achieved using locations determined from a laterally homogeneous (1-D) velocity model, with or without station corrections (statics). The coupling between hypocenter and velocity structure is a prime aspect of Local Earthquake Tomography (Thurber, 1992).

2 Data & Methodology

To image the seismically active western Tibet, we perform the state-of-the-art earthquake relocation technique and the double difference seismic tomography approach curated by Zhang and Thurber (2003), commonly known as tomoDD. For this analysis, we used continuous waveform data recorded by a seismic array deployed across western Tibet, operating from July 2007 to May 2011 (Razi et al., 2014). Only seismic events recorded by three or more stations were considered to ensure high-quality data for both P- and S-waves. These seismic stations were spatially distributed within the latitude interval 30°N to 34°N and longitude interval 79°E to 84°E (Fig. 1), with a mean elevation of 4500 m. The stringent selection criteria of using 180 seconds waveform of the earthquake event recorded at least four seismic stations allowed only 124 well-constrained earthquakes. The initial location was en-

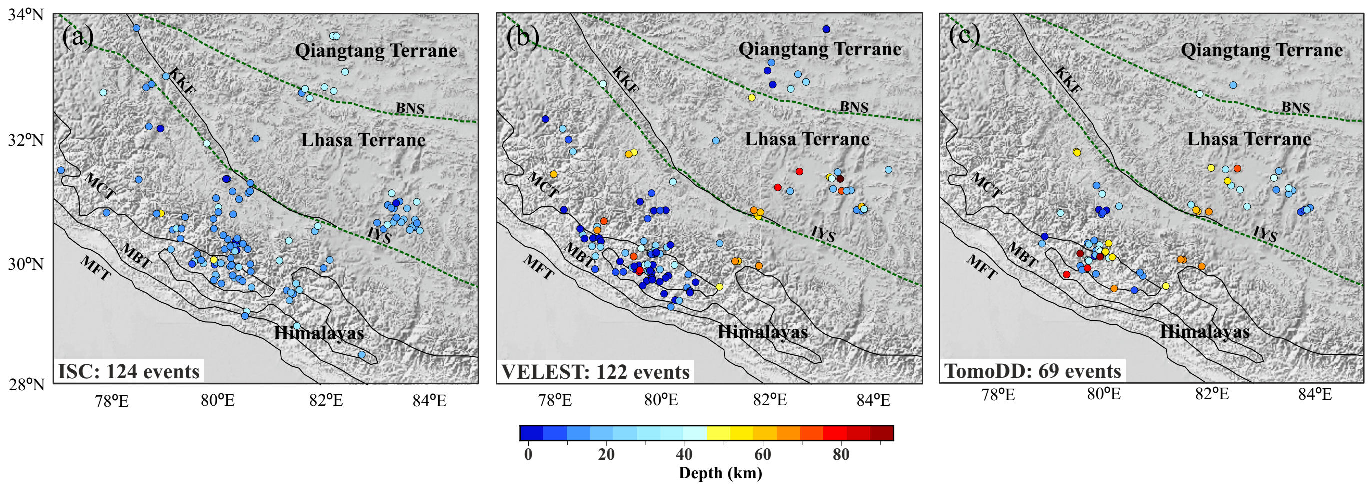

Figure 3 Initial earthquake locations as observed from (a) ISC catalogue, (b) relocated earthquakes obtained from velest and (c) final relocated earthquakes as observed from TomoDD.

abled by SEISAN algorithm (Havskov and Ottemoller, 1999). The high quality dataset ensures the quality of the velocity models (Zhang and Thurber, 2003). This process is derived from the double-difference (DD) method of earthquake location proposed by Waldhauser (2001) and Waldhauser and Ellsworth (2000).

TomoDD uses relative and absolute arrival data that are simultaneously gathered at station pairs for two events that are relatively close together (approximately 100 km). Instead of relying solely on modified picks, this method has the advantage of providing both relative and absolute arrival times together with their quality values, which helps to preserve important information. Thus, it generates absolute locations instead of relative ones and removes the need for basic assumptions about path anomalies or ray path geometries (Zhang and Thurber, 2003). The dataset includes 871 P-wave arrivals, 673 S-wave arrivals, 3349 P-wave differential periods, and 2748 S-wave differential timings. Earthquake relocation and tomography were performed with a 1-D initial velocity model, the accuracy of which partly determines the final results. According to Razi et al. (2014), P-wave velocities vary from 5.7-6.4 km/s across the surface to the mid-crust, and 8.0-8.2 km/s at upper mantle depths up to 130 km. Thus, we adopted the P-wave velocities 5.8 km/s, 6.2 km/s, 6.2 km/s and 8.1 km/s at 3 km, 18 km, 39 km, and 75 km respectively obtained after six iterations through VELEST (Kissling et al., 1995) as our starting point for inversion. VELEST not only facilitates the precise localization of seismic events (Fig. 2) but also enables the derivation of a detailed velocity structure along with station residuals. It is to be noted here, that shallow 3D velocity model may have artifacts from near surface features directly beneath the stations, which can be addressed by applying necessary station corrections. However, we observe that the station corrections did not seem to alter the recovered shallow model, and thus have been omitted.

For 1-D velocity model, the VELEST program simultaneously varies the hypocenters and inverts them using a five-layer model based on LITHO1.0 as the starting model. In order to confirm the robustness of the solution and prevent becoming trapped in local minima, the velocity model from VELEST with RMS < 0.3 s was utilized as subsequent starting model for 3D inversion using TomoDD (Fig. 3), ensuring a stable solution. The initial velocities at each grid node were interpolated using a trilinear interpolation technique (Eberhart-Phillips and Michael, 1993). The S-wave model was derived by assuming a constant P-wave (Vp) to S-wave (Vs) velocity ratio, fixed at 1.7 up to 18 km, 1.73 up to 75 km and 1.8 across the upper mantle, an assumption based on prior studies by Razi et al. (2014). Since enhanced velocity models can lead to significant improvements in earthquake locations, the TomoDD technique simultaneously resolves velocity models (Vp, Vs) together with the relocation of the earthquake events.

We utilized a Cartesian model with $55 \times 55 \times 30$ grid-nodes extending in x, y and z directions respectively. The central node (0 km) is positioned at 33°N and 81°E. 27 node points spread in the east, west, north and south directions respectively from the central node, i.e., along the x and y axes spaced at 30 km increment. The z-axis nodes are uniformly spaced at 3 km intervals down to 60 km depth (23rd node), after which the spacing increases extending till 130 km (30th node). An additional z-axis node is placed at -5 km and -10 km depth to account for the complex topography of the region and to incorporate air-quakes from the iterative relocation algorithm. Preliminary earthquake locations indicate that most events occur between 40-60 km depth closer to the Himalayas, with some shallower events around 15-20 km depth across the BNS. The grid was extended beyond the existing event range to accommodate the overshooting raypaths frequently produced by the algorithm.

After running the tomoDD algorithm, we accounted for path anomaly biases between earthquake events, ultimately yielding 84 high-quality relocated events (Fig. 3). We managed the weighting between absolute and differential time data using a hierarchical approach, where the weighting parameters are designed to capture broad-scale velocity heterogeneity, while the differential data refine near-source struc-

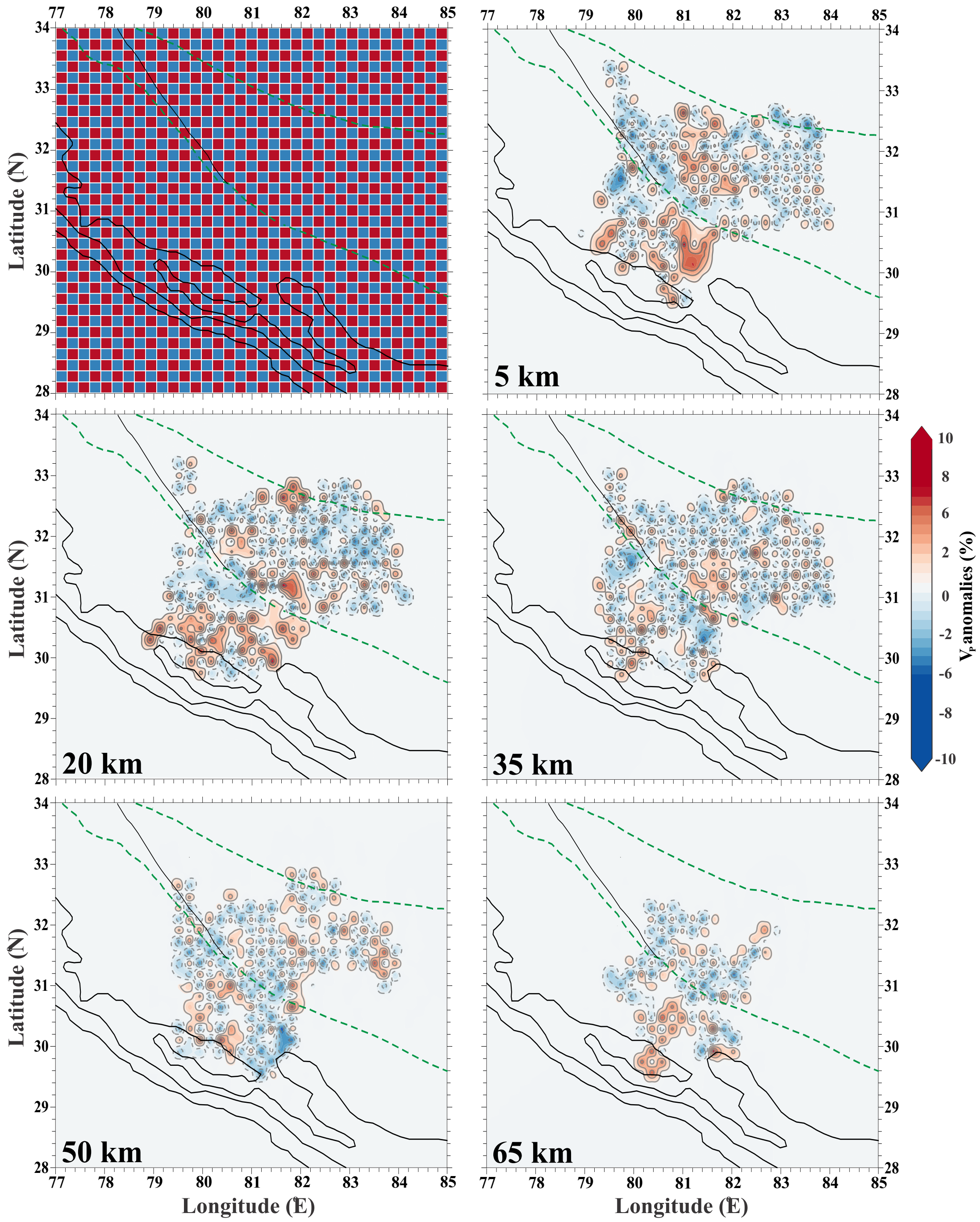

Figure 4 Checkerboard test conducted on a 20 km × 20 km grid across the study area. The first panel on the top left represents the input model, while subsequent panels represent the checkerboard output at various depths as indicated in each panel.

tures (Eberhart-Phillips and Michael, 1993; Thurber and Eberhart-Phillips, 1999). The initial velocities specified at each grid were interpolated throughout the model using a bilinear interpolation technique (Eberhart-Phillips and Michael, 1993; Thurber and Eberhart-Phillips, 1999). Throughout the process, a large number of damping values were tested. For the initial iteration, a large damping value of 1000 was used to suppress the effect of artifacts, followed by lower damping values, to improve the resolution of the model. For the consecutive final iterations, the change in misfit became less than 0.01%. Finally, we generated 3-D tomographic models of the crustal Vp, and Vs within a 1100 × 1100 km^2 region. To ensure the resolution of the tomographic images, we also perform a simple 20 km × 20 km checkerboard resolution test with 10% velocity anomalies (Fig. 4) along with Derivative Weighted Sum (DWS) analysis (Fig. S1).

2.1 Derivative Weighted Sum

The resolution test is a crucial method to assess how accurately tomographic images can reveal crustal heterogeneity. In this study, we also used the DWS to evaluate the quality and reliability of the inverted velocity structure. DWS values quantify the extent to which each node within the study area is sampled by seismic ray paths. The concept is similar to the seismic fold in active seismic methods, based on the distribution of hit counts. Higher DWS values indicate better sampling of ray paths in that grid; however, the azimuthal distribution of seismic ray paths must also be considered (Fang and Zhang, 2014).

The lower limit of DWS values is ideally zero, signifying that no rays have traversed the grid, causing the grid to output the background velocity. Since multiple clusters were identified after 3D inversion, with each cluster containing mutually separated events, a grid may experience rays originating from more than one cluster. Consequently, the DWS value for a particular grid is the sum of the contributions from each earthquake cluster.

The tomographic images achieve their highest resolution within the latitude range of 29° to 33° N and the longitude range of 78.5° to 84° E, with average DWS values ranging from 70 to 80 for P-waves (Fig. S1). It is evident that DWS values are densely concentrated around the geometry of the installed stations, but at greater depths, they align with the orientations of the earthquake hypocenter locations. In the vicinity of a cluster centroid, DWS values are relatively high because the energy source is located there. More ray paths pass through these nearby grids due to reflection and refraction.

3 Results

3.1 Relocated Earthquake Cluster & Velocity Anomalies

The TomoDD algorithm, which utilizes the absolute and differential arrival times of the seismic signals, provides a more accurate means of calculating the location of events and the velocity structure beneath the subsurface compared to the traditional absolute arrival time tomography (Zhang and Thurber, 2006). Five earthquake clusters are identified throughout the study region (Table 1). The largest cluster, consisting of 57 events, is located south of the KKF, concentrated near the Main Central Thrust (MCT), Main Boundary Thrust (MBT), and Main Frontal Thrust (MFT) (Fig. S2) at an approximate depth of 42 km. The second and third largest clusters, containing 11 and 10 earthquake events, respectively, are located within the Lhasa block (Fig. S1, Table 1). Although the third cluster lies at a deeper depth of around 62 km near the tail end of the KKF, the second cluster is located at the eastern margin of the study area in the Lhasa block. The remaining two clusters are located south of the Qiangtang block and south of the KKF (Fig. S2). The tomoDD method greatly improved the epicenter and hypocenter locations, reducing the RMS errors by up to ten times compared to our initial earthquake location analysis using SEISAN. 90% of the original earthquake locations had RMS errors in the range of 0.1-0.2 s, with a substantial improvement, as currently ∼70% of the relocated earthquakes have RMS errors within the range of 0.5 to 1.5 ms.

The crustal P-wave velocity anomaly extends up to 12% (Fig. 5), while S-wave velocity anomalies reach up to 6% in the upper crust and 10% in the lower crust (Fig. S3). The mean P-wave velocity is 5.80 km/s at a depth of 15 km, increasing to an average of 6.60 km/s at depths of up to 60 km. Similarly, the mean S-wave velocity is 3.35 km/s at depths of up to 15 km, 3.36 km/s at 36 km, and 3.56 km/s at depths of up to 75 km. The anomalies are more pronounced in the central part of the study region and gradually diminish toward its edges. The abrupt changes in velocity structure between depths of 65-75 km, with an average velocity of 7.8 km/s at 75 km depth, confirm the presence of the Moho.

Cluster no.	Lat (°N)	Lon (°E)	Dep (km)	No. of EQ
Cluster 1	30.60	79.98	42.13	57
Cluster 2	30.87	83.85	17.41	11
Cluster 3	30.85	81.83	61.97	10
Cluster 4	32.82	82.51	19.77	4
Cluster 5	31.79	79.58	52.87	2

Table 1 Cluster centroid information of the relocated earthquakes (EQ).

3.2 Attributes of the 3D Model

This study presents a quantitative analysis of the velocity structure beneath the subsurface of the Himalayas and western Tibet. A common trend is easily noticeable: a high P-wave velocity zone or a fast anomaly is located in the Himalayan terrane. Another significant feature is the presence of a slow anomaly that aligns with the KKF (A1, Fig. 5).

At 20 km depth, the southeastern and northeastern regions of the Lhasa block exhibit a fast anomaly of ∼8-10% (A2, Fig. 5), while the Qiangtang block shows evidence of a slow anomaly. The boundary between the fast and slow anomalies is more distinct in the eastern part of the Lhasa block, with deviations of approximately 2.5% from the mean velocity, compared to the western part (Fig. 5). The slow anomaly extends across the region bounded by 80.5°E to 82.5°E and 31°N to 32.25°N, persisting to a depth of up to 65 km.

A prominent low V_p anomaly (A3) is observed drifting downward in the depth section along 32°N latitude (Fig. 6) and 82°E longitude (Fig. 7). This slow velocity anomaly predominantly affects the southwestern portion of the Lhasa block. At the terminus of the KKF, a distinct fast anomaly (up to 2% higher than the mean velocity) is identified, accompanied by slow anomaly fragments (up to 5% slower than the mean velocity) to the north (Fig. 7).

Overall, the slower anomaly along the KKF (A4, Fig. 7) contrasts sharply with the stable fast anomaly of the Indian plate below the Himalayas (A5, Fig. 7), which is up to 10% higher than the mean velocity. The southern Qiangtang block is characterized by a uniform slow anomaly, whereas the Lhasa block features a fast anomaly at its easternmost margin. Additionally, a high anomaly is observed dipping northeast beneath the plateau.

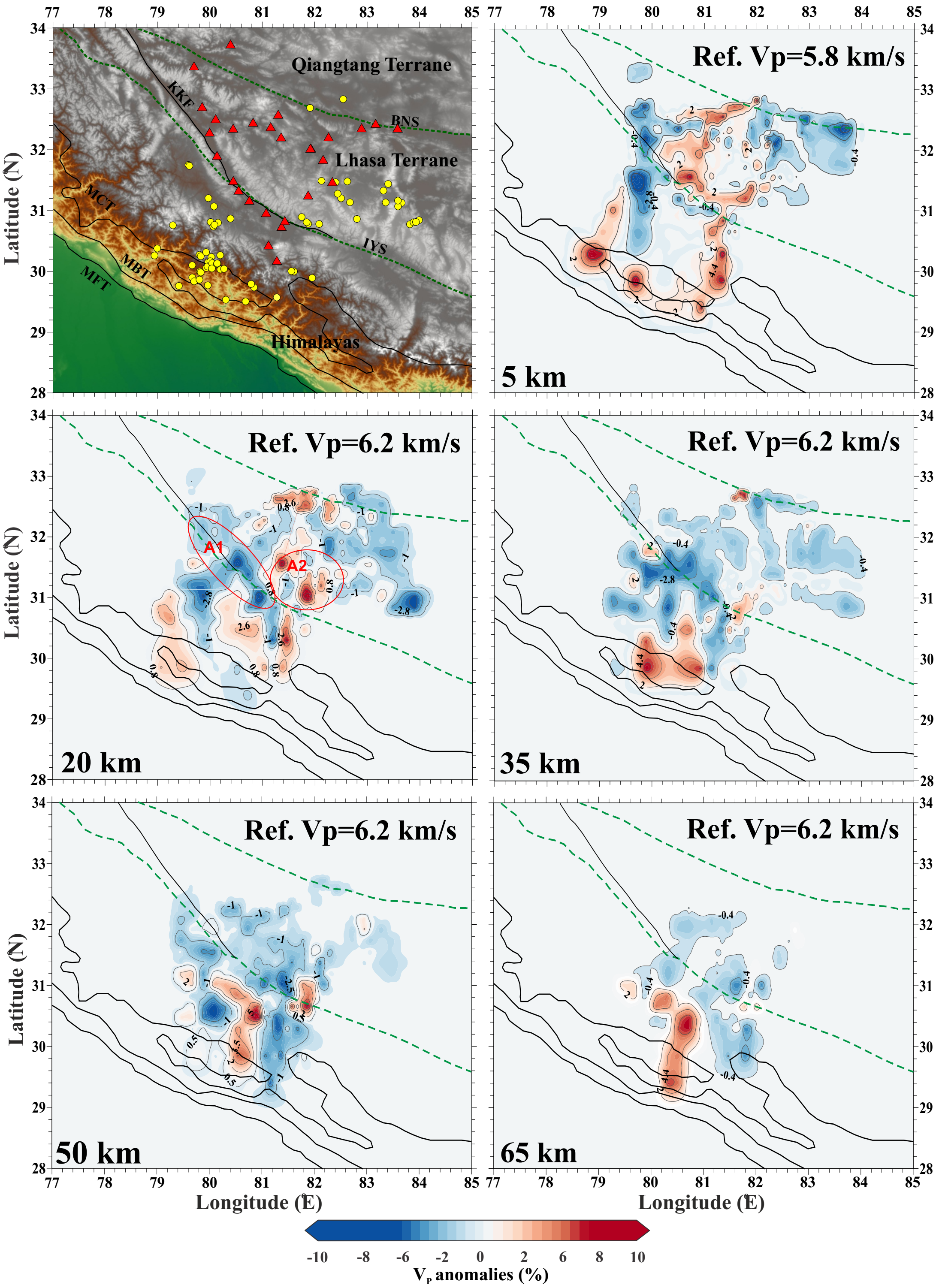

Figure 5 P-wave velocity anomaly tomographic images across the study area at the depth indicated at the bottom left corner of each panel. The reference Vp is indicated at the top right corner of each slice.

4 Discussion

Our study provides a detailed velocity model of the subsurface beneath western Tibet and the Himalayan region. The mean velocity of the 20 km thick upper crust is estimated to be 5.80 km/s, while the 60 km thick lower crust exhibits a mean velocity of 6.20 km/s. This finding deviates from the results of Razi et al. (2014), who reported a mean crustal P-wave velocity of 6.20 km/s for the entire crust. However, the broader patterns observed in our study are consistent with their findings. Some of the notable features evident from our study are: (1) A prominent slow anomaly predominantly affecting the southwestern portion of the Lhasa block. (2) A distinct fast anomaly at the terminus of the KKF (up to 2% higher than the mean velocity), accompanied by slow anomaly fragments (up to 5% slower than the mean velocity) moving to the north. (3) Stable fast anomalies in the Himalayan crust, with velocities 5–10% higher in the upper crust and 2–5% higher in the lower crust (Fig. 6).

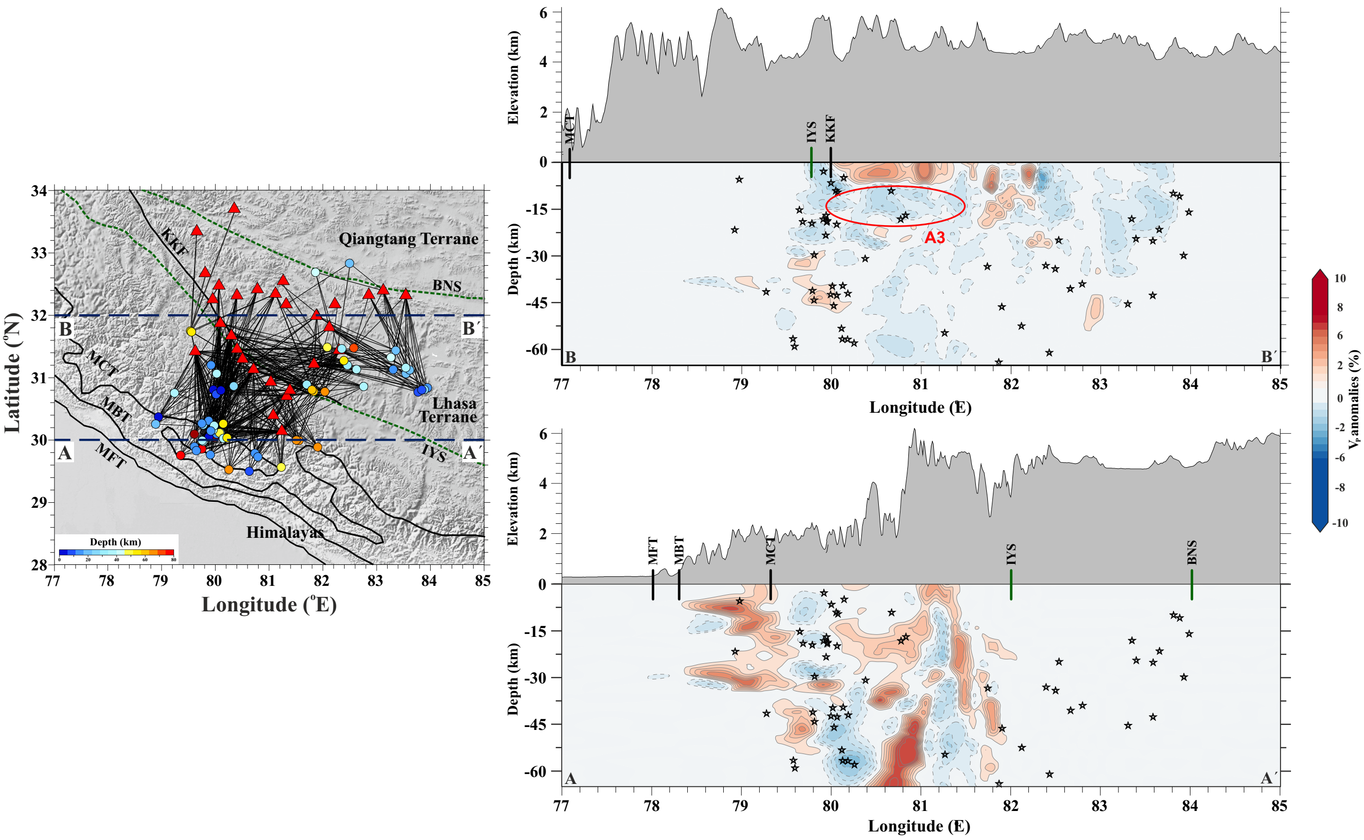

Figure 6 Vertical cross-section of the velocity structures (Vp) along the latitudes 30.0°N (Profile AA') and 32.0°N (Profile BB'). The color scale represents the percentage deviation of velocity anomaly from the mean value. The topographic map is also represented to understand the changes in elevation and tectonics along the profile length. The inset map on the left represents the study area with the profiles marked.

The crust beneath the Himalayas display stable fast anomalies. These high-velocity zones strongly suggest the underthrusting of the Indian lithosphere beneath the Himalayan region. The transition from slower material beneath the Lhasa block to faster crust beneath the Himalayas likely marks the plate boundary between the Indian and Eurasian subduction zones. Previous studies have debated the presence of a pronounced low-velocity channel in the mid-to-lower crust, with depths ranging from 20–40 km (Rapine et al., 2003), 30–50 km (Kind et al., 1996), or 30–70 km (Cotte et al., 1999). In this context, the channel-flow model proposed by Nelson et al. (1996) posits that the Greater Himalayan Sequence (GHS) results from the continuous extrusion of molten middle crust. This process occurs as the Indian crust subducts northward beneath the Lhasa terrane, leading to heating and partial melting. The resulting molten material forms a southward-directed return flow, driven by the gravitational potential energy of the elevated Tibetan Plateau. Figs. 6 and 7, which depict the southward movement of the slow anomaly (A3), likely represent this flow of molten crustal material.

Our study challenges the prevailing notion of significant crustal material exchange between the Indian and Eurasian plates, as proposed by the channel flow model (Klemperer, 2006). Instead, our findings are consistent with recent studies, such as those by Caldwell et al. (2013) and Leech (2008), which describe the KKF as affecting the crust primarily. The observed low velocities (5.5–6.0 km/s) beneath the Lhasa block cannot be attributed solely to the ongoing collision between the Indian and Eurasian plates. Instead, it likely results from processes linked to the pre-collision formation of the Lhasa block. Notably, the separation between faster-moving material beneath the Himalayas and slower-moving material beneath the Lhasa block (Fig. 6) does not follow a strictly vertical path. Instead, it exhibits a noticeable slope towards the north and east (Profile DD', Fig. 7). This configuration suggests a thrust-type relationship, where the Lhasa block rests within a hanging wall. This observation departs from the well-documented strike-slip fault motion along the KKF and indicates a more complex stress transfer mechanism in the region (Styron et al., 2011). Furthermore, the reduced velocity along the KKF could result from increased fracturing, the presence of fluids, or a combination of both, altering the physical properties of the crustal material along the fault (Sibson, 1994).

However, the overall crustal Vp of western Tibet is lower than in the remaining parts of the plateau (Klemperer, 2006). Previous studies have documented that the Qiangtang and Lhasa terranes experience an average P-wave velocity of approximately 6.0 km/s, which is lower than the continental global average velocity of 6.45 km/s (Haines et al., 2003). Seismic wave velocities are influenced by lithology, fluid content, and temperature distribution. The higher the SiO_2 content in a rock, the lower its seismic velocity (Christensen and

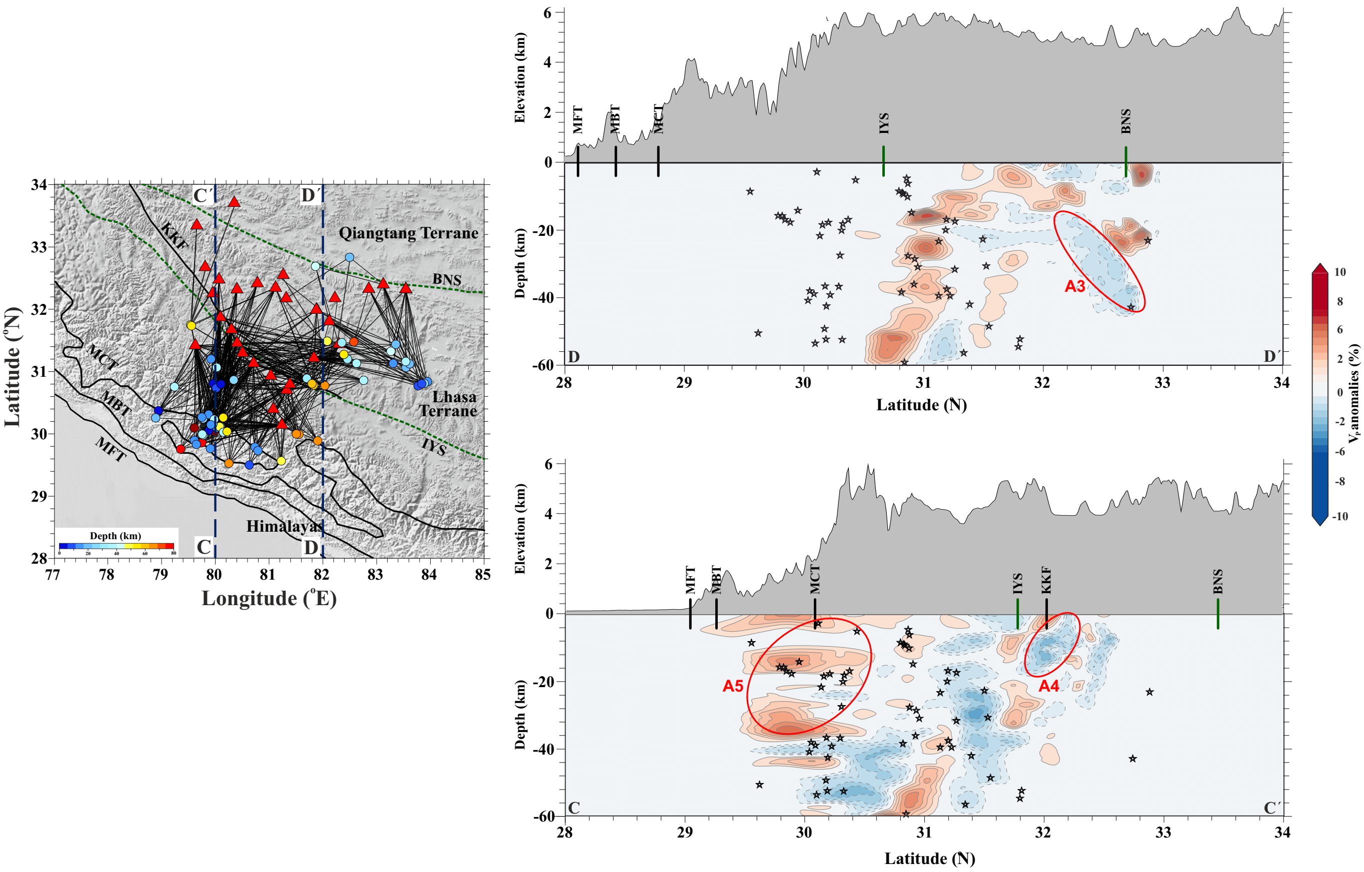

Figure 7 Vertical cross-section of the velocity structures (Vp) along the longitudes 80.0°E (Profile CC') and 82.0°E (Profile DD'). The color scale represents the percentage deviation of velocity anomaly from the mean value. The topographic map is also represented to understand the changes in elevation and tectonics along the profile length. The inset map on the left represents the study area with the profiles marked.

Mooney, 1995), which results from a low melting point and consequently a considerable reduction in the rock strength. A crust with lower velocity is indicative of weaker strength. Without considering abrupt critical crustal settings and detailed geological rock properties, the cause of such low crustal Vp (up to 5% lesser than the mean velocity) can be explained by the lower crust being bypassed by lateral flow, leading to partial melting (Haines et al., 2003).

The observed low crustal V_p(up to 5% lower than the mean velocity) can be attributed to lateral flow within the lower crust, resulting in partial melting (Haines et al., 2003). This phenomenon does not need abrupt tectonic settings or detailed geological rock properties but reflects broader crustal processes impacting the region. While the Vp is significantly low, the Vp/Vs ratio remains normal to high, supporting the theory of partial melt in the crust as suggested by Tian et al. (2005), Vergne et al. (2002). In our study, we observed the presence of higher Vp anomaly fragments (up to 5% greater than the mean velocity) in the lower crust of the plateau beyond a depth of 45 km, around the latitude range 31-32°N and longitudinal range 81.5° - 83.5°E. DeCelles et al. (2002) suggest that the high Vp layer beneath the plateau is Indian cratonic lower crust. A deep seismic study led by Zhang et al. (2011) also suggests that the leading edge of the subducted Indian lithosphere reaches the northern margin of the Tibetan Plateau at the Tarim Basin at 80°E. Additionally, if the lower crust attains a higher velocity, the mid and upper crust must have a considerably low Vp.

Earlier, Schulte-Pelkum et al. (2005) found evidence of unusually high velocities beneath the higher Himalayas. This transformative process typically involves the subduction of Indian crust beneath the plateau. The identification of high-velocity layers at the crust-mantle interface, as evidenced by studies such as Huang et al. (2009), Schulte-Pelkum et al. (2005), and Nábělek et al. (2009), aligns with the characteristics of transform boundaries. These observations (Fig. 8) are particularly significant, as they aid in delineating the extent of the Indian lithosphere.

5 Conclusions

In this study, our objective is to unravel the intricate velocity structure beneath the Himalayas and western Tibet using local earthquake tomography through the TomoDD algorithm. The key highlights of the study are as follows:

- The relocated earthquake data predominantly clusters south of the KKF within the Indian lithosphere. This distribution suggests that the Indian lithosphere is more seismically active compared to the relatively stable Tibetan Plateau.

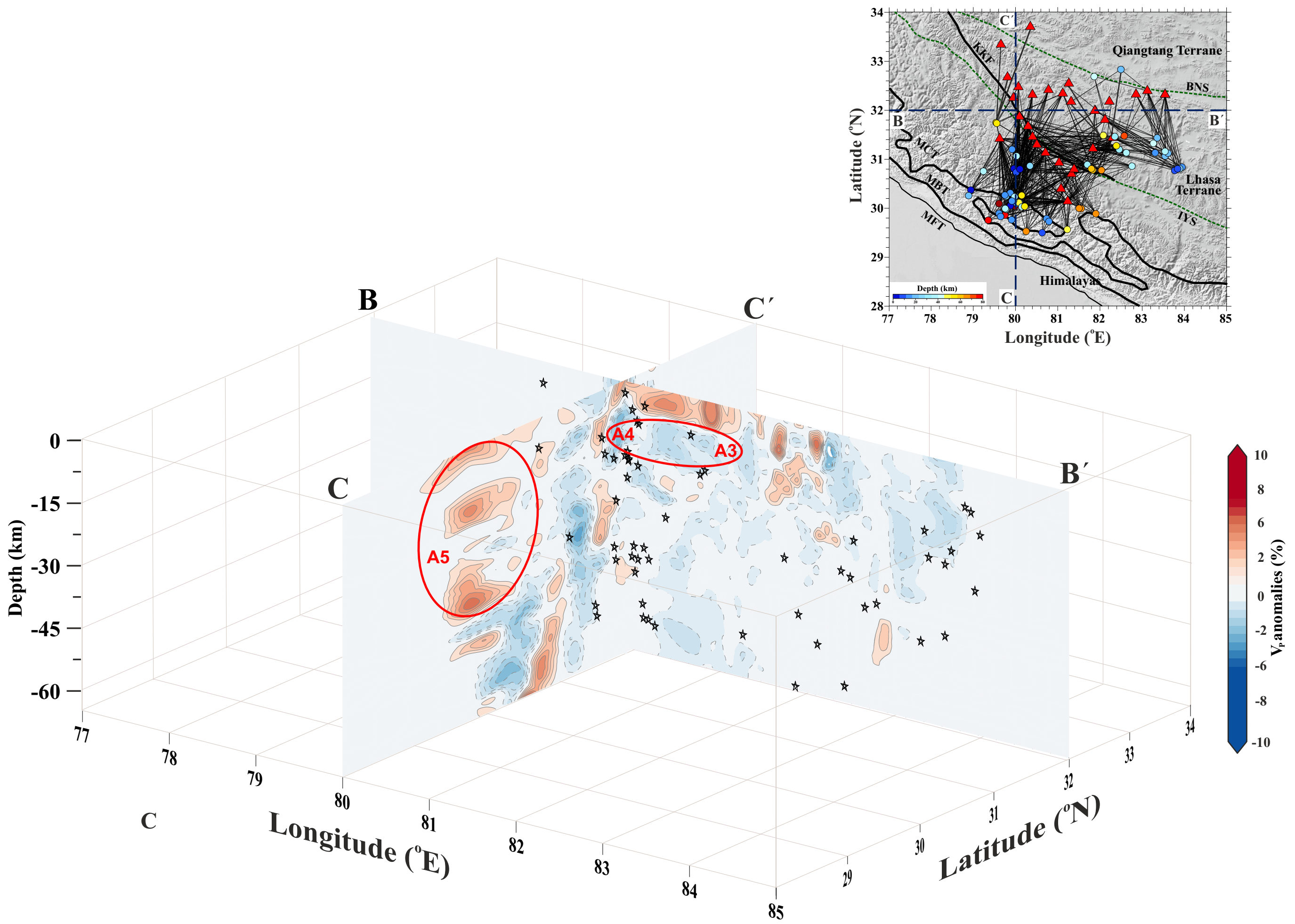

Figure 8 Schematic representation of the velocity anomaly variation observed at the intersection with the Karakoram Fault. The relocated earthquakes (black stars) mostly coincide with the low-velocity anomaly.

- The crust beneath the Himalayan range is characterized by a stable fast anomaly. Distinct features along the KKF and the Indus-Yarlung Suture demarcate the subduction boundary between the Indian and Eurasian lithospheres. The northeastward-dipping KKF appears to play a crucial role in differentiating the velocity distributions.
- Evidence of partial melting in the crust of the Tibetan Plateau, causing elevated temperatures in the lower crust and upper mantle, likely leads to a reduction in P-wave velocity. A channel flow, transporting crustal material southward, is evident throughout much of the crust. Partial eclogitization contributes to a stable high V_p in the crust across the higher Himalayas.
- Prominent fast anomalies are observed at greater depths along the western margin of the Lhasa block, while a slow anomaly is evident in its eastern part. A stable slow V_p anomaly is noted in the Qiangtang block, which could possibly be attributed to weaker resolution across the region.

Acknowledgements

The article is part of the student-master dissertation of Arghya Kusum Dey. The Department of Applied Geophysics, Indian Institute of Technology (ISM) Dhanbad is gratefully acknowledged for the computational resources. Niptika Jana acknowledges Prof. Clifford Thurber for providing the tomoDD algorithm package for use. The authors would further like to thank 2 anonymous reviewers and editor Chiara Civiero for the detailed suggestions that have significantly improved the manuscript.

Data and code availability

Supporting Information includes Figures S1–S3. The seismic array network dataset used in this paper is available from Razi et al. (2014), Razi et al. (2016). Information of local earthquake catalog has been obtained from Biswas and Singh (2020a) and Biswas and Singh (2020b).

Competing interests

The authors declare no competing interests.

References

Alsdorf, D., Makovsky, Y., Zhao, W., Brown, L., Nelson, K., Klemperer, S., Hauck, M., Ross, A., Cogan, M., Clark, M., et al. INDEPTH (International Deep Profiling of Tibet and the Himalaya) multichannel seismic reflection data: Description and availability. *Journal of Geophysical Research: Solid Earth*, 103(B11): 26993–26999, 1998. doi: 10.1029/98JB01078.

Basuyau, C., Diament, M., Tiberi, C., Hetényi, G., Vergne, J., and Peyrefitte, A. Joint inversion of teleseismic and GOCE gravity data: application to the Himalayas. *Geophysical Journal International*, 193(1):149–160, 2013. doi: 10.1093/gji/ggs110.

Bilham, R. et al. Earthquakes in India and the Himalaya: tectonics, geodesy and history. *Annals of GEOPHYSICS*, 2004. doi: 10.4401/ag-3338.

Biswas, R. and Singh, C. Attenuation of high frequency body waves in the crust of western Tibet. *Physics of the Earth and Planetary Interiors*, 298:106323, 2020a. doi: 10.1016/j.pepi.2019.106323.

Biswas, R. and Singh, C. An investigation of regional variations of coda wave attenuation in western Tibet. *Journal of Seismology*, 24(6):1235–1254, 2020b. doi: 10.1007/s10950-020-09929-0.

Caldwell, W. B., Klemperer, S. L., Lawrence, J. F., Rai, S. S., et al. Characterizing the Main Himalayan Thrust in the Garhwal Himalaya, India with receiver function CCP stacking. *Earth and Planetary Science Letters*, 367:15–27, 2013. doi: 10.1016/j.epsl.2013.02.009.

Christensen, N. I. and Mooney, W. D. Seismic velocity structure and composition of the continental crust: A global view. *Journal of Geophysical Research: Solid Earth*, 100(B6):9761–9788, 1995. doi: 10.1029/95JB00259.

Cotte, N., Pedersen, H., Campillo, M., Mars, J., Ni, J., Kind, R., Sandvol, E., and Zhao, W. Determination of the crustal structure in southern Tibet by dispersion and amplitude analysis of Rayleigh waves. *Geophysical Journal International*, 138(3): 809–819, 1999. doi: 10.1046/j.1365-246x.1999.00927.x.

DeCelles, P. G., Robinson, D. M., and Zandt, G. Implications of shortening in the Himalayan fold-thrust belt for uplift of the Tibetan Plateau. *Tectonics*, 21(6):12–1, 2002. doi: 10.1029/2001TC001322.

Dubey, A. K., Singh, A., Kumar, M. R., Jana, N., Sarkar, S., Saikia, D., and Singh, C. Tomographic imaging of the plate geometry beneath the Arunachal Himalaya and Burmese subduction zones. *Geophysical Research Letters*, 49(8):e2022GL098331, 2022. doi: 10.1029/2022GL098331.

Eberhart-Phillips, D. and Michael, A. J. Three-dimensional velocity structure, seismicity, and fault structure in the Parkfield region, central California. *Journal of Geophysical Research: Solid Earth*, 98(B9):15737–15758, 1993. doi: 10.1029/93JB01029.

Fang, H. and Zhang, H. Wavelet-based double-difference seismic tomography with sparsity regularization. *Geophysical Journal International*, 199(2):944–955, 2014. doi: 10.1093/gji/ggu305.

Gilligan, A., Priestley, K. F., Roecker, S. W., Levin, V., and Rai, S. The crustal structure of the western Himalayas and Tibet. *Journal of Geophysical Research: Solid Earth*, 120(5):3946–3964, 2015. doi: 10.1002/2015JB011891.

Haines, S. S., Klemperer, S. L., Brown, L., Jingru, G., Mechie, J., Meissner, R., Ross, A., and Wenjin, Z. INDEPTH III seismic data: From surface observations to deep crustal processes in Tibet. *Tectonics*, 22(1), 2003. doi: 10.1029/2001TC001305.

Havskov, J. and Ottemoller, L. SEISAN earthquake analysis software. *Seismological Research Letters*, 70(5):532–534, 1999. doi: 10.1785/gssrl.70.5.532.

Huang, G.-C. D., Wu, F. T., Roecker, S. W., and Sheehan, A. F. Lithospheric structure of the central Himalaya from 3-D tomographic imaging. *Tectonophysics*, 475(3-4):524–543, 2009. doi: 10.1016/j.tecto.2009.06.023.

Jaiswal, N., Singh, C., and Singh, A. Crustal structure of western Tibet revealed by Lg attenuation tomography. *Tectonophysics*, 775:228245, 2020. doi: 10.1016/j.tecto.2019.228245.

Jaiswal, N., Singh, C., Sarkar, S., Tiwari, A. K., and Jana, N. Pg attenuation tomography beneath western Tibet. *Journal of Seismology*, 26(3):531–543, 2022. doi: 10.1007/s10950-022-10086-9.

Jia, M. The Transformation of Tibetan Identity. 2015.

Kapp, P., Murphy, M. A., Yin, A., Harrison, T. M., Ding, L., and Guo, J. Mesozoic and Cenozoic tectonic evolution of the Shiquanhe area of western Tibet. *Tectonics*, 22(4), 2003. doi: 10.1029/2001TC001332.

Kapp, P., Yin, A., Harrison, T. M., and Ding, L. Cretaceous-Tertiary shortening, basin development, and volcanism in central Tibet. *Geological Society of America Bulletin*, 117(7-8):865–878, 2005. doi: 10.1130/B25595.1.

Kapp, P., DeCelles, P. G., Gehrels, G. E., Heizler, M., and Ding, L. Geological records of the Lhasa-Qiangtang and Indo-Asian collisions in the Nima area of central Tibet. *Geological Society of America Bulletin*, 119(7-8):917–933, 2007. doi: 10.1130/B26033.1.

Kind, R., Ni, J., Zhao, W., Wu, J., Yuan, X., Zhao, L., Sandvol, E., Reese, C., Nabelek, J., and Hearn, T. Evidence from earthquake data for a partially molten crustal layer in southern Tibet. *Science*, 274(5293):1692–1694, 1996. doi: 10.1126/science.274.5293.1692.

Kissling, E. Geotomography with local earthquake data. *Reviews of Geophysics*, 26(4):659–698, 1988. doi: 10.1029/RG026i004p00659.

Kissling, E., Kradolfer, U., and Maurer, H. Program VELEST user's guide-Short Introduction. *Institute of Geophysics, ETH Zurich*, 1995.

Klemperer, S. L. Crustal flow in Tibet: geophysical evidence for the physical state of Tibetan lithosphere, and inferred patterns of active flow. *Geological Society, London, Special Publications*, 268(1):39–70, 2006. doi: 10.1144/GSL.SP.2006.268.01.03.

Klemperer, S. L., Kennedy, B. M., Sastry, S. R., Makovsky, Y., Harinarayana, T., and Leech, M. L. Mantle fluids in the Karakoram fault: Helium isotope evidence. *Earth and Planetary Science Letters*, 366:59–70, 2013. doi: 10.1016/j.epsl.2013.01.013.

Leech, M. L. Does the Karakoram fault interrupt mid-crustal channel flow in the western Himalaya? *Earth and Planetary Science Letters*, 276(3-4):314–322, 2008. doi: 10.1016/j.epsl.2008.10.006.

Molnar, P. and Tapponnier, P. Cenozoic tectonics of Asia: effects of a continental collision. *science*, 189(4201):419–426, 1975. doi: 10.1126/science.189.4201.419.

Murphy, M., Yin, A., Harrison, T., Durr, S., Ryerson, F., and Kidd, W. Did the Indo-Asian collision alone create the Tibetan plateau? *Geology*, 25(8):719–722, 1997. doi: 10.1130/0091-7613(1997)025.

Nábělek, J., Hetényi, G., Vergne, J., Sapkota, S., Kafle, B., Jiang, M., Su, H., Chen, J., Huang, B.-S., and Team, t. H.-C. Underplating in the Himalaya-Tibet collision zone revealed by the Hi-CLIMB experiment. *Science*, 325(5946):1371–1374, 2009. doi: 10.1126/science.1167719.

Nelson, K. D., Zhao, W., Brown, L., Kuo, J., Che, J., Liu, X., Klemperer, S., Makovsky, Y., Meissner, R., Mechie, J., et al. Partially molten middle crust beneath southern Tibet: Synthesis of project INDEPTH results. *science*, 274(5293):1684–1688, 1996. doi: 10.1126/science.274.5293.1684.

Rapine, R., Tilmann, F., West, M., Ni, J., and Rodgers, A. Crustal structure of northern and southern Tibet from surface wave dispersion analysis. *Journal of Geophysical Research: Solid Earth*, 108(B2), 2003. doi: 10.1029/2001JB000445.

Razi, A. S., Levin, V., Roecker, S. W., and Huang, G.-c. D. Crustal and uppermost mantle structure beneath western Tibet using seismic traveltime tomography. *Geochemistry, Geophysics, Geosystems*, 15(2):434–452, 2014. doi: 10.1002/2013GC005143.

Razi, A. S., Roecker, S. W., and Levin, V. The fate of the Indian lithosphere beneath western Tibet: Upper mantle elastic wave speed structure from a joint teleseismic and regional body wave tomographic study. *Physics of the Earth and Planetary Interiors*, 251:11–23, 2016. doi: 10.1016/j.pepi.2015.12.001.

Royden, L. H., Burchfiel, B. C., and van der Hilst, R. D. The geological evolution of the Tibetan Plateau. *science*, 321(5892): 1054–1058, 2008. doi: 10.1126/science.1155371.

Schulte-Pelkum, V., Monsalve, G., Sheehan, A., Pandey, M., Sapkota, S., Bilham, R., and Wu, F. Imaging the Indian subcontinent beneath the Himalaya. *Nature*, 435(7046):1222–1225, 2005. doi: 10.1038/nature03678.

Shen, Z.-K., Lü, J., Wang, M., and Bürgmann, R. Contemporary crustal deformation around the southeast borderland of the Tibetan Plateau. *Journal of Geophysical Research: Solid Earth*, 110 (B11), 2005. doi: 10.1029/2004JB003421.

Sibson, R. H. Crustal stress, faulting and fluid flow. *Geological Society, London, Special Publications*, 78(1):69–84, 1994. doi: 10.1144/GSL.SP.1994.078.01.07.

Singh, A., Singh, C., and Kennett, B. A review of crust and upper mantle structure beneath the Indian subcontinent. *Tectonophysics*, 644:1–21, 2015. doi: 10.1016/j.tecto.2015.01.007.

Singh, A., Ravi Kumar, M., Mohanty, D. D., Singh, C., Biswas, R., and Srinagesh, D. Crustal structure beneath India and Tibet: New constraints from inversion of receiver functions. *Journal of Geophysical Research: Solid Earth*, 122(10):7839–7859, 2017. doi: 10.1002/2017JB013946.

Styron, R. H., Taylor, M. H., and Murphy, M. A. Oblique convergence, arc-parallel extension, and the role of strike-slip faulting in the High Himalaya. *Geosphere*, 7(2):582–596, 2011. doi: 10.1130/GES00606.1.

Thurber, C. and Eberhart-Phillips, D. Local earthquake tomography with flexible gridding. *Computers & Geosciences*, 25(7): 809–818, 1999. doi: 10.1016/S0098-3004(99)00007-2.

Thurber, C. H. Hypocenter-velocity structure coupling in local earthquake tomography. *Physics of the Earth and Planetary Interiors*, 75(1-3):55–62, 1992. doi: 10.1016/0031-9201(92)90117-E.

Tian, X., Wu, Q., Zhang, Z., Teng, J., and Zeng, R. Joint imaging by teleseismic converted and multiple waves and its application in the INDEPTH-III passive seismic array. *Geophysical Research Letters*, 32(21), 2005. doi: 10.1029/2005GL023686.

Valli, F., Arnaud, N., Leloup, P. H., Sobel, E. R., Mahéo, G., Lacassin, R., Guillot, S., Li, H., Tapponnier, P., and Xu, Z. Twenty million years of continuous deformation along the Karakorum fault, western Tibet: A thermochronological analysis. *Tectonics*, 26 (4), 2007. doi: 10.1029/2005TC001913.

Vergne, J., Wittlinger, G., Hui, Q., Tapponnier, P., Poupinet, G., Mei, J., Herquel, G., and Paul, A. Seismic evidence for stepwise thickening of the crust across the NE Tibetan plateau. *Earth and Planetary Science Letters*, 203(1):25–33, 2002. doi: 10.1016/S0012-821X(02)00853-1.

Waldhauser, F. HypoDD-A program to compute double-difference hypocenter locations. Technical report, 2001. doi: 10.3133/ofr01113.

Waldhauser, F. and Ellsworth, W. L. A double-difference earthquake location algorithm: Method and application to the northern Hayward fault, California. *Bulletin of the seismological society of America*, 90(6):1353–1368, 2000. doi: 10.1785/0120000006.

Wittlinger, G., Farra, V., and Vergne, J. Lithospheric and upper mantle stratifications beneath Tibet: New insights from Sp conversions. *Geophysical Research Letter*, 31(19), 2004. doi: 10.1029/2004GL020955.

Yin, A. and Harrison, T. M. Geologic evolution of the Himalayan-Tibetan orogen. *Annual review of earth and planetary sciences*, 28(1):211–280, 2000. doi: 10.1146/annurev.earth.28.1.211.

Yuan, X., Ni, J., Kind, R., Mechie, J., and Sandvol, E. Lithospheric and upper mantle structure of southern Tibet from a seismological passive source experiment. *Journal of Geophysical Research: Solid Earth*, 102(B12):27491–27500, 1997. doi: 10.1029/97JB02379.

Zhang, H. and Thurber, C. Double-difference tomography: The method and its application to the Hayward fault, California. *Bulletin of the Seismological Society of America*, 93(5):1875–1889, 2003. doi: 10.1785/0120020190.

Zhang, H. and Thurber, C. Development and applications of double-difference seismic tomography. *pure and applied geophysics*, 163:373–403, 2006. doi: 10.1007/s00024-005-0021-y.

Zhang, Z., Deng, Y., Teng, J., Wang, C., Gao, R., Chen, Y., and Fan, W. An overview of the crustal structure of the Tibetan plateau after 35 years of deep seismic soundings. *Journal of Asian Earth Sciences*, 40(4):977–989, 2011. doi: 10.1016/j.jseaes.2010.03.010.